

Effect of electron scattering mechanisms on the transport properties of GaAs microstructures in the “energy quasiballistic” regime

Yu. V. Dubrovskii, I. A. Larkin, and S. V. Morozov

Institute of Problems of the Technology of Microelectronics and Especially Pure Materials, Academy of Sciences of the USSR

(Submitted 10 December 1990)

Zh. Eksp. Teor. Fiz. **99**, 1827–1835 (June 1991)

Nonlinear features have been observed experimentally in the electron transport in GaAs microstructures at applied voltages below 10 mV at low temperatures ($T < 100$ K). These features stem from an increase in the electron temperature T_e along the structure, over a distance shorter than the energy relaxation length. In this case there is essentially no energy relaxation in the course of the motion of the electrons (the “energy quasiballistic regime”). When the voltage across the sample becomes comparable in magnitude to the energy of an optical phonon in electron volts, an inelastic-loss mechanism comes into play, and T_e reaches saturation. The observed nonlinearities disappear. The kinetic equation is solved in the hydrodynamic approximation for these experimental conditions. Good agreement is found with experiment. The temperature dependence of the momentum relaxation time of the electron gas can be extracted directly from the current-voltage characteristics in the energy quasiballistic regime.

1. As the geometric dimensions of samples decrease to values on the order of the length scales in the solid, e.g., the mean free path l_p , the screening length, and the de Broglie wavelength, it becomes possible to observe several new physical phenomena, e.g., ballistic transport and resonant tunneling.^{1,2} In each of these cases there is a length scale which is of fundamental importance to an interpretation of the experimental results.

In this paper we are reporting a study of the electron transport and the heating of the electron system in GaAs microstructures in the case in which the length L of the structure satisfies $l_p \ll L < l_e$, where l_e is the energy relaxation length. We have observed a new short-channel effect, which is associated with a variation of the electron temperature T_e along the channel, over a distance shorter than l_e . This effect is also associated with saturation of T_e when the applied voltage is on the order of the energy of an optical phonon, $\hbar\Omega_0$. In the region with the nonuniform temperature distribution, the electrons move with essentially no energy loss. We call this situation an “energy quasiballistic regime.”

Our experimental results are presented in Sec. 2. In Sec. 3 we adopt the hydrodynamic approximation to discuss a theoretical model for explaining the results. We make some quantitative estimates. In Sec. 4 we compare this model with the experimental data. The particular shape of the current-voltage characteristics in the energy quasiballistic regime depends on the particular functional dependence of the momentum relaxation time τ_p of the electrons on T_e . It thus becomes possible to identify the predominant scattering mechanisms in our structures. These topics are the subject of Sec. 5.

2. The GaAs test samples had the topology of field-effect transistors with Schottky-barrier gates. The gates of the particular transistors which we studied had lengths $L = 0.5, 5, 10,$ and $500 \mu\text{m}$; their width was $100 \mu\text{m}$. All the transistors were fabricated on epitaxial films with $N_d - N_a \approx 10^{17} \text{ cm}^{-3}$. For the length $L = 0.5 \mu\text{m}$, at least, the condition $L \ll l_e$ holds well^{3,4} at $T \leq 50$ K.

The differential resistance $R_d = dV_c/dI_c$ and/or the

differential conductance $\sigma_d = dI_c/dV_c$ of the channel in the transistor was measured as a function of the voltage V_c applied between the drain and the source. The measurements were carried out at sample temperatures from $T = 4.2$ K up to room temperature. In most cases, the fixed gate voltage V_g was chosen so that the channel remained conducting, but its resistance was much higher than the resistances of the source-channel and channel-drain regions and also much higher than the resistances of the contacts. Under these conditions, these other resistances can be ignored. At any rate, as the blocking voltage applied to the gate is increased and as the resistance of the channel increases, the nonlinear behavior of the resistance is simply amplified.

Figure 1, a and b, shows illustrative experimental curves for various temperatures, for $L = 0.5 \mu\text{m}$ and $L = 10 \mu\text{m}$. We note the following features of these results. (1) The differential resistance falls off rapidly with increasing applied voltage, up to $V_c \approx 10$ mV, at which the change slows down considerably. (2) At $T = 4.2$ K, the experimental curves for $L = 0.5, 5,$ and $10 \mu\text{m}$ are essentially identical in shape at a given voltage scale. For $L = 500 \mu\text{m}$, we have $R_d = \text{const}$ at all temperatures. (3) With increasing temperature, the functional dependence $R_d = f(V_c)$ weakens, essentially disappearing at a certain T^* . A similar nonlinear behavior of the conductance was observed in GaAs/Al_xGa_{1-x}As heterostructures in Ref. 5, but we are not convinced by the interpretation offered there, which made use of space-charge-limited currents.

3. To describe our experimental results and to derive quantitative estimates, we use the hydrodynamic approximation. In the steady state, the kinetic equation describing the electron current in the channel is (in the standard notation)

$$\mathbf{v} \nabla f(\mathbf{v}, \mathbf{r}) + \frac{e\mathbf{E}}{m^*} \frac{\partial f(\mathbf{v}, \mathbf{r})}{\partial \mathbf{v}} = S_{ee} + S_{imp} + S_{eph}, \quad (1)$$

where S_{ee} , S_{imp} , and S_{eph} are the electron-electron, electron-impurity, and electron-phonon collision integrals. Since the cross section for the scattering by impurity centers is a power function of the energy of the particle, and since the electron

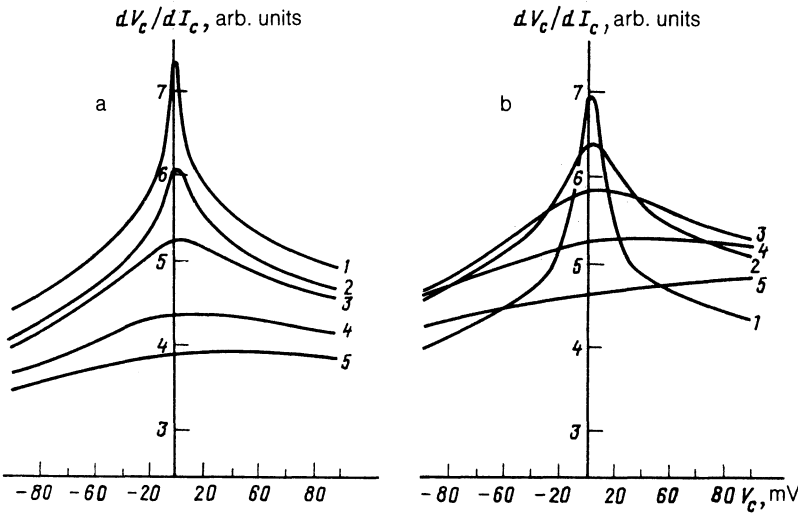


FIG. 1. Differential resistance of the channel versus the applied voltage at various sample temperatures. a: $L = 0.5 \mu\text{m}$. 1— $T = 4.2 \text{ K}$; 2—28; 3—70; 4—110; 5—150. b: $L = 10 \mu\text{m}$. 1— $T = 4.2 \text{ K}$; 2—28; 3—42; 4—55; 5—70.

drift time near the gate ($\sim 10^{-8}$ – 10^{-9} s) is much longer than the electron-electron scattering time ($\sim 10^{-13}$ s), the solution of Eq. (1) is approximately a shifted Maxwellian distribution with an electron temperature $T_e(\mathbf{r})$:

$$f(v, \mathbf{r}) = \frac{n_e m^{*3/2}}{[2\pi T_e(\mathbf{r})]^{3/2}} \exp\left[-\frac{m^*(v-U)^2}{2T_e(\mathbf{r})}\right].$$

Here we are assuming that the drift velocity U is constant along the channel. This assumption follows from the current conservation law and from the circumstance that the electron density n_e and the channel thickness d can be assumed to remain constant as a function of the coordinate x along the channel under our experimental conditions. Specifically, we have $n_e(x) = \text{const}$ since the Debye screening length at $n_e \approx 10^{17} \text{ cm}^{-3}$ and $L_D \sim 10 \text{ nm}$ is much shorter than the channel thickness $d \sim 100$ – 250 nm in our experiments. We set $d(x) = \text{const}$ because the typical applied voltages, $V_c \sim 10 \text{ mV}$, are much lower than the voltages ($\sim 1 \text{ V}$) which would be required to block the channel. We assume that T_e depends only on the coordinate along the channel (x). Integrating (1) over d^3v with weights of v_x and $m^*v^2/2$, as in Ref. 6, we find the system of equations

$$-\frac{\partial T_e}{\partial x} + e \frac{\partial \varphi}{\partial x} = \frac{m^*U}{\tau_p(T_e)}, \quad (2)$$

$$-\frac{5}{2} \frac{\partial T_e}{\partial x} + e \frac{\partial \varphi}{\partial x} = \frac{P_{ph}(T_e)}{U}, \quad (3)$$

where $\tau_p(T_e)$ is the momentum relaxation time, $P_{ph}(T_e)$ is the rate at which the electrons lose energy to phonons, and φ is the electrostatic potential.

To solve Eqs. (2) and (3), we need to specify the functional dependences $\tau_p(T_e)$ and $P_{ph}(T_e)$, which are determined by the predominant scattering mechanisms. At low temperatures, $\tau_p(T_e)$ is determined by scattering by ionized impurity centers. In a Boltzmann gas it is given by^{3,7}

$$\tau_p(T_e) = \bar{\tau}_p (T_e / \hbar\Omega_0)^{3/2}.$$

For $P_{ph}(T_e)$, we consider only the scattering caused by optical phonons. The time scale of the energy relaxation due to acoustic phonons, $\tau_{eac} \sim 10^{-8}$ s (Refs. 3 and 4), is shorter than or on the order of the time taken by the electrons to traverse the gate region in short-channel structures. A

threshold is involved in the scattering by optical phonons:³

$$P_{ph}(T_e) = \frac{\hbar\Omega_0}{\tau_0^*} \exp\left(-\frac{\hbar\Omega_0}{T_e}\right),$$

where $\hbar\Omega_0 = 36 \text{ mV}$ is the energy of the optical phonons. The quantity τ_0^* in the different limiting cases ($\tau_0 \ll \tau_{ee}$ or $\tau_0 \gg \tau_{ee}$) is $\max(\tau_0, \tau_{ee})$, where $\tau_0 = 0.14 \text{ ps}$ is the optical-phonon emission time, and τ_{ee} is the effective electron-electron collision time. Under our experimental conditions, τ_{ee} is on the order of τ_0 (Ref. 3), so for definiteness we set $\tau_0^* = 0.2 \text{ ps}$ in the calculations.

We would like to point out some features which follow from Eqs. (2) and (3). As long as T_e is much smaller than $\hbar\Omega_0$, we can ignore the term on the right in Eq. (3); the electrons move with essentially no energy loss. This is the regime which we are calling the “energy quasiballistic regime.” It can evidently occur at low temperatures in short-channel structures which satisfy the condition $L \leq l_e$. It follows from Eq. (3) that the electron temperature follows the potential distribution, $T_e(x) \approx 2/5e\varphi(x)$, and increases linearly with an increase in the applied voltage. The derivative $\partial\varphi/\partial x$ thus decreases with x because of the increase in T_e and the decrease in the scattering by the impurity centers. The result is a decrease in the differential resistance which would be observed experimentally. With a further increase in V_c , a potent energy-loss mechanism, involving optical phonons, comes into play, and the electron temperature reaches saturation. The curve of $R_d = f(V_c)$ smooths out. In other words, as V_c is increased, the quantity l_e first becomes comparable to L and then smaller than it. As the sample temperature is raised, l_e again decreases, and the effect fades away, first for $L = 10 \mu\text{m}$ and then for $L = 5$ and $0.5 \mu\text{m}$.

We can estimate the temperature T^* corresponding to the change in regime. From (2) and (3) we have

$$\frac{3}{2} \frac{\partial T_e}{\partial x} = \frac{m^*U}{\tau_p(T_e)} - \frac{P_{ph}(T_e)}{U}. \quad (4)$$

Setting $eV_c \sim \hbar\Omega_0$, we find, with logarithmic accuracy, the temperature corresponding to $\partial T_e/\partial x \approx 0$:

$$T^* \approx \hbar\Omega_0 / \ln\left(\frac{m^*L^2}{\tau_0^* \tau_p \hbar\Omega_0}\right). \quad (5)$$

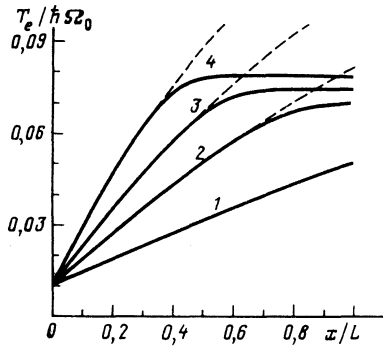


FIG. 2. Calculated profile of the electron temperature along the coordinate for $L = 5 \mu\text{m}$ and $T = 4.2 \text{ K}$. 1— $eV_c / \hbar\Omega_0 = 0.06$; 2—0.11; 3—0.15; 4—0.21. The dashed curves were calculated without consideration of phonon scattering ($P_{ph} = 0$).

The effects described here can evidently be observed at $T \leq T^*$. Setting $\tau_p \approx 0.2 \text{ ps}$, we find $T^* \approx 65 \text{ K}$ for $L = 0.5 \mu\text{m}$, while for $L = 5$ and $10 \mu\text{m}$ we find $T^* \approx 38$ and 34 K , respectively. These results agree fairly well with the experimental data (Fig. 1, a and b). At $L = 500 \mu\text{m}$, the scattering by acoustic phonons is important. In this case we have $l_e \ll L$ for any V_c , and no such effects are observed.

Equations (2) and (3) describe the transport of electrons both in the energy quasiballistic regime [$P_{ph}(T_e) \ll m^*U^2/\tau_p(T_e)$] and in the transition to the dissipative regime [$P_{ph}(T_e) \approx m^*U^2/\tau_p(T_e)$]. Numerical integration of Eqs. (2) and (3) led to the behavior shown in Figs. 2–4. Since the electron gas in GaAs at $n_e \approx 10^{17} \text{ cm}^{-3}$ is degenerate, although the Fermi energy E_F is relatively small, we used the following interpolation:

$$\tau_p(T_e) = \bar{\tau}_p \left[\left(\frac{E_F}{\hbar\Omega_0} \right)^{1/2} + \left(\frac{T_e}{\hbar\Omega_0} \right)^{1/2} \right].$$

In the calculations we set $E_F = 0.1\hbar\Omega_0$ and $\bar{\tau}_p = 2 \text{ ps}$; we took the electron temperature at the entrance to the channel to be equal to the sample temperature, $T = 0.01\hbar\Omega_0$.

It was assumed that the carriers leave the channel and go into a large electron reservoir, with large geometric dimensions and/or a high Fermi energy, e.g., a heavily doped ohmic contact, which does not contribute significantly to the resistance of the sample. In this case the drift velocity U decreases sharply, and the electron temperature relaxes quickly to the lattice temperature by virtue of the acoustic phonons. Allowing for the thermal electron diffusion away

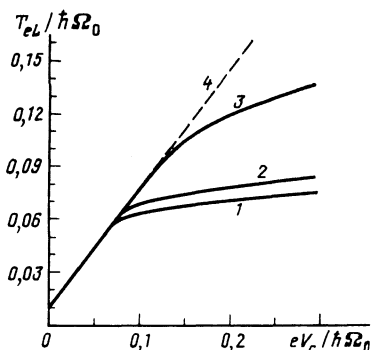


FIG. 3. Calculated dependence of the electron temperature at the end of the channel, T_{eL} , on the applied voltage for $T = 4.2 \text{ K}$. 1— $L = 10 \mu\text{m}$; 2—5; 3—0.5. Curve 4 was calculated for $P_{ph} = 0$.

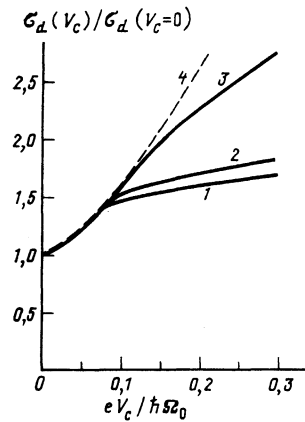


FIG. 4. Calculated behavior of the differential conductance as a function of the applied voltage at $T = 4.2 \text{ K}$. 1— $L = 10 \mu\text{m}$; 2—5; 3—0.5. Curve 4 was calculated for $P_{ph} = 0$.

from the point of the channel with the T_e maximum, we used the effective electrochemical potential $\mu = e\varphi - T_e$ in plotting the curves in Figs. 2–4. According to Eq. (2), $\mu(x)$ remains essentially constant after exit from the channel, and its total change over the length of the sample is equal to V_c . The distinction between μ and the ordinary electrochemical potential is discussed in Ref. 7.

4. For convenience in comparing the theoretical and experimental results, we have shown in Fig. 5 (curve 1) the experimental dependence $\sigma_d = f(V_c)$ (the measurements carried out in magnetic fields are discussed in the following section of this paper). In general, the theoretical curves reproduce the characteristic features of the experimental curves. Specifically, the shape of the theoretical curves in Fig. 4 is the same as that of the experimental curves in Figs. 1 and 5 (curve 1). The onset of saturation in the case $L = 0.5 \mu\text{m}$ is more gradual (see curve 3 in Fig. 4 and Fig. 1a). The relative changes in the differential conductance from $V_c = 0$ up to the inflection point on the theoretical and experimental curves are nearly identical. For $L = 5 \mu\text{m}$, for example (curve 2 in Fig. 4 and curve 1 in Fig. 5), they are about 60%.

Let us compare the values of T^* and V_c^* corresponding to the change in regime. For definiteness we assume that V_c^* corresponds to the inflection point on the $\sigma_d = f(V_c)$ curves. Experimentally we have $V_c^* \approx 10\text{--}12 \text{ mV}$. The corresponding theoretical value is $V_c^* \approx 3.6\text{--}4.5 \text{ mV}$. In order to

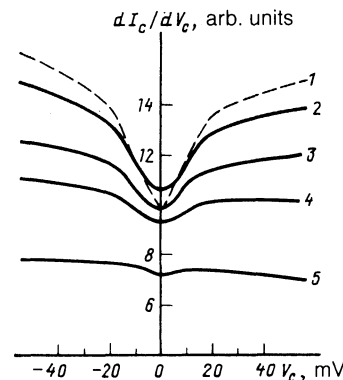


FIG. 5. Differential conductance versus the applied voltage in various magnetic fields at $L = 5 \mu\text{m}$ and $V_g = -1.9 \text{ V}$. 1— $H = 0 \text{ kOe}$; 2—10; 3—20; 4—30; 5—40.

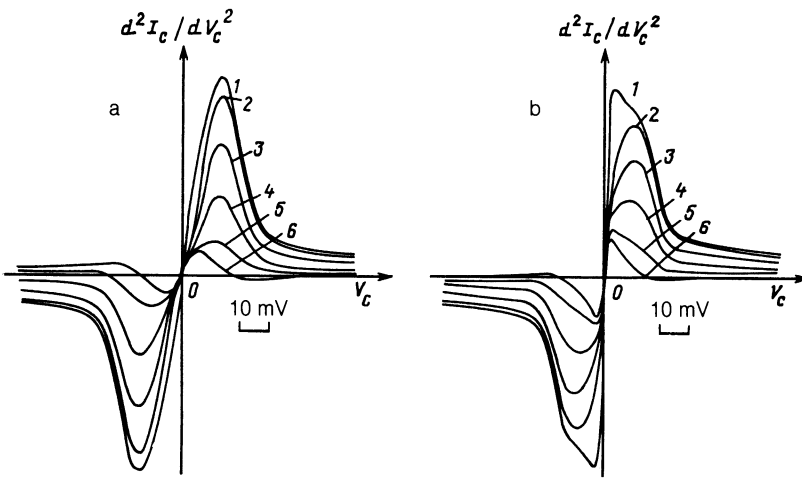


FIG. 6. Curves of d^2I_c/dV_c^2 versus the applied voltage in various magnetic fields (directed perpendicular to the plane of the sample), with $L = 5 \mu\text{m}$ and $T = 4.2 \text{ K}$. 1— $H = 0$ kOe; 2—6; 3—15; 4—25; 5—38; 6—50. a: $V_g = 0.0 \text{ V}$. b: $V_g = -2.0 \text{ V}$.

find T^* from the experimental data, we work from the temperature dependence shown in Fig. 1, a and b. We take T^* to be the sample temperature at which the average slope of the $R_d = f(V_c)$ curve at $V_c < V_c^*$ becomes approximately equal to the slope of the curve found for $T = 4.2 \text{ K}$ and $V_c > V_c^*$. For $L = 0.5$ and $10 \mu\text{m}$, we have $T^* = 70$ and 35 K , respectively. The theoretical value of T^* for $L = 0.5 \mu\text{m}$ is about 50 K , while that for $L = 10 \mu\text{m}$ is 25 K . The estimate of T^* from (5) lies between the theoretical and experimental values for the various sample lengths.

Equation (5) describes a logarithmically weak dependence of T^* on the length of the sample for $L > 0.1 \mu\text{m}$. We believe that this point explains the approximately equal values observed experimentally for V_c^* at the various values of L . The reason why the calculated values of T^* are small is the relation $\tau_0^* \ll m^*L^2/(\tau_p T^*)$. The preexponential factor calculated in Ref. 8 is slightly lower than the value which we used, but under our experimental conditions the difference is less than an order of magnitude. Our calculation shows that the corresponding increase in τ_0^* by an order of magnitude would improve the agreement with experiment slightly, but T^* would increase by only about 20%.

The greatest discrepancy between experiment and theory is seen in the comparison of the V_c^* values. The apparent reason for this discrepancy is that the model proposed here describes a channel which is uniform and of constant width; it ignores the actual geometry of the structure. Perhaps non-equilibrium effects in the channel-contact transition regions should be taken into account more carefully. To do this would require a self-consistent numerical solution of a two-dimensional Poisson equation and a kinetic equation, with all scattering mechanisms, in particular, scattering by acoustic phonons, being taken into account. The model of the present paper incorporates only the fundamental points, so one can explicitly see the most characteristic features of the experimental results.

5. In this section we take a more detailed look at the nature of the nonlinear resistance in our samples in the energy quasiballistic regime [$V_c < V_c^*$ and $P_{ph}(T_e) \approx 0$]. For this regime, using $\sigma(T_e) = e^2 n \tau_p(T_e)/m^*$ and $I_c = enSU$, we can write Eqs. (2) and (3) as

$$\frac{\partial \mu}{\partial x} \sigma(T_e) = \frac{eI_c}{S},$$

$$\frac{3}{2} \frac{\partial T_e}{\partial x} = \frac{\partial \mu}{\partial x},$$

where $\sigma(T_e)$ is the longitudinal conductance corresponding to T_e , and S is the cross-sectional area of the channel. Integrating these equations, and then differentiating the first of them with respect to V_c , we finally find

$$\sigma_d \propto \frac{\partial I_c}{\partial V_c} \frac{L}{S} = \sigma(T_{eL}) \propto \tau_p(T_{eL}),$$

$$T_{eL} - T = \tau_p^2 / 3eV_c,$$

where T_{eL} is the electron temperature at the end of the channel, at the point of the T_e maximum. The differential conductance measured in the energy quasiballistic regime is thus directly proportional to the local conductance at the end of the channel, and there is the possibility in principle of determining $\sigma(T_e)$ directly from the experimental behavior. If scattering by an ionized impurity is the governing factor, we would expect $\sigma_d \propto V_c^{3/2}$. Since the exponent here is close to one, it would be easier to study the dependence $d^2I_c/dV_c^2 = f(V_c)$.

For definiteness below, we assume a sample with $L = 5 \mu\text{m}$ at $T = 4.2 \text{ K}$. Figure 6a, b shows experimental results on $d^2I_c/dV_c^2 = f(V_c)$ for gate voltages $V_g = 0.0 \text{ V}$ and -2.0 V . The energy quasiballistic regime prevails at $V_c < 10 \text{ mV}$. In this region, the behavior of curve 1 in Fig. 6a is qualitatively different from that of curve 1 in Fig. 6b. While curve 1 in Fig. 6a rises smoothly with V_c , that in Fig. 6b is discontinuous at $V_c = 0$ and descends with increasing V_c . In the case $V_g = 0.0 \text{ V}$, the thickness of the conducting channel is $d \approx 250 \text{ nm}$, while at $V_g = -2.0 \text{ V}$ it is $d \approx 70 \text{ nm}$.

Measurements in magnetic fields might cast some light on the reason for this evolution of the experimental curves with decreasing channel thickness. Figure 7 shows the conductance of the channel versus the magnetic field in the absence of a heating electric field. In weak magnetic fields we observe a negative magnetoresistance, which becomes more obvious as the blocking voltage applied to the gate is increased. This behavior is determined by weak localization.⁹ As the blocking voltage on the gate is raised, the channel thickness becomes smaller than the phase relaxation length L_ϕ , and there is a smooth transition to localization corrections of a quasi-2D nature.¹⁰ For $N_d \approx 10^{17} \text{ cm}^{-3}$ in GaAs at

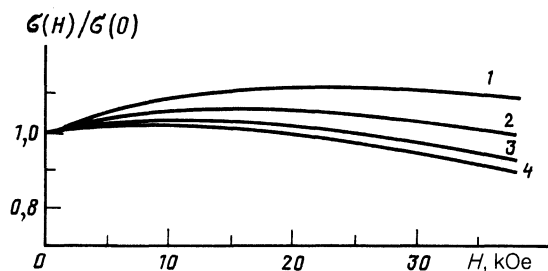


FIG. 7. Conductance of the channel versus the magnetic field for various gate voltages ($L = 5 \mu\text{m}$). 1— $V_g = -3.0 \text{ V}$; 2— -2.5 ; 3— -1.5 ; 4— 0.0 .

$T = 4.2 \text{ K}$ we have $L_\varphi \approx 0.3\text{--}0.4 \mu\text{m}$ (Ref. 11). In the quasi-2D case, the localization corrections to the conductance are $\Delta\sigma \propto -\ln(L_\varphi/l_p)$, where L_φ falls off in a power-law fashion with the temperature.

We wish to stress that Eqs. (2) and (3) were derived without any special assumptions regarding the nature of the relaxation of the electron momentum. For this reason, τ_p in Eq. (2) is proportional to the local conductance $\sigma = \sigma_{cl} + \Delta\sigma$, where σ_{cl} is the classical local conductance. Consequently, the change in the localization corrections with the temperature in sufficiently thin channels is predominant; it is this circumstance which leads to a dependence $d^2I_c/dV_c^2 \propto V_c^{-1}$ under energy quasiballistic conditions.

A weak magnetic field can suppress weak-localization effects. The curves for a narrow channel actually transform in this case to the shape characteristic of a wide channel, in which the predominant mechanism is classical scattering by impurity centers (Fig. 6, a and b). Figure 8 shows curves of d^2I_c/dV_c^2 versus the magnetic field H for various applied voltages. These results demonstrate the disruption of the weak localization with increasing temperature T_e . At low applied voltages, for which the temperature of the electron gas is low, there is a region of a relatively sharp decay of the curves in the magnetic fields characteristic of weak localization. With increasing applied voltage, T_e rises, and the weak localization is disrupted. As a result, the experimental curves become smoother. When the localization corrections are unimportant, the magnetic field can be dealt with by replacing $\tau_p(T_e)$ in Eqs. (2) and (3) by

$$\tau_{p\text{eff}}(T_e) = \frac{\tau_p(T_e)}{1 + \omega_c^2 \tau_p^2(T_e)},$$

where ω_c is the cyclotron frequency. This conclusion is in

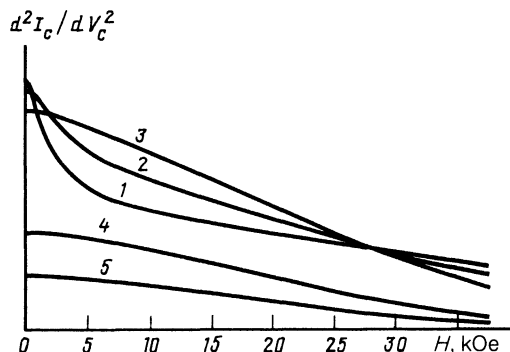


FIG. 8. Plot of d^2I_c/dV_c^2 versus the magnetic field for various applied voltages for $L = 5 \mu\text{m}$ and $V_g = -2.0 \text{ V}$. 1— $V_c = 3.0 \text{ mV}$; 2— 5.6 ; 3— 10.2 ; 4— 20.5 ; 5— 30.2 .

qualitative agreement with the evolution of the experimental curves in Figs. 5–8.

On the whole, this study shows that the nonlinearity of the resistance observed in GaAs short-channel structures can be described fairly well by the energy quasiballistic model. It has been shown that the energy quasiballistic regime presents us with a new way to study the behavior of the relaxation time of the electron gas as a function of its temperature.

We wish to thank I. B. Levinson, V. A. Tulin, and Yu. N. Khanin for useful discussions. We also thank V. G. Lapin for furnishing the test samples.

¹ H. Schmid, S. A. Rishton, D. P. Kern *et al.*, *J. Vac. Sci. Technol.* **B 6**, 122 (1988).

² M. Heiblum, M. I. Nathan, D. S. Thomas, and C. M. Knodler, *Phys. Rev. Lett.* **55**, 2200 (1985).

³ V. F. Gantmakher and I. B. Levinson, *Carrier Scattering in Metals and Semiconductors*, Nauka, Moscow, 1984. (North-Holland, Amsterdam, 1987.)

⁴ Yu. V. Dubrovskii and V. V. Krasnyak, *Fiz. Tekh. Poluprovodn.* **21**, 170 (1987) [*Sov. Phys. Semicond.* **21**, 104 (1987)].

⁵ T. H. Thornton, M. Pepper, H. Ahmet *et al.*, *Electron. Lett.* **22**, 247 (1986).

⁶ S. I. Braginskii, in *Reviews of Plasma Physics*, Gosatomizdat, Moscow, 1963, p. 163 (Consultants Bureau, New York, 1965).

⁷ E. M. Lifshitz and L. P. Pitaevskii, *Physical Kinetics*, Nauka, Moscow, 1978 (Pergamon, Oxford, 1981).

⁸ S. E. Esipov, *Zh. Eksp. Teor. Fiz.* **90**, 2247 (1986) [*Sov. Phys. JETP* **63**, 1319 (1986)].

⁹ E. A. Polyanskaya and Yu. V. Shmartsev, *Fiz. Tekh. Poluprovodn.* **23**, 3 (1989) [*Sov. Phys. Semicond.* **23**, 1 (1989)].

¹⁰ D. J. Newson, C. M. McFadden, and C. M. Pepper, *Philos. Mag.* **B 52**, 437 (1985).

¹¹ O. V. Emel'yanenko, T. S. Lagunova, and T. A. Polyanskaya, *Pis'ma Zh. Eksp. Teor. Fiz.* **36**, 199 (1982) [*JETP Lett.* **36**, 246 (1982)].

Translated by D. Parsons